Supporting Information

Aerogel Templating on Functionalized Fibers of Nanocellulose Networks

Thanh-Dinh Nguyen,[a] Wadood Y. Hamad,[b] and Mark J. MacLachlan[a,*]

[a]Department of Chemistry, University of British Columbia, 2036 Main Mall, Vancouver, British Columbia V6T 1Z1, Canada

[b]FPInnovations, 2665 East Mall, Vancouver, British Columbia V6T 1Z4, Canada

*Corresponding author: mmaclach@chem.ubc.ca

1. Experimental Section

Chemicals: Aqueous suspensions of cellulose nanocrystals (CNCs) were prepared according to a literature procedure by sulfuric acid hydrolysis of commercial bleached kraft wood pulp.[1,2] The physical dimensions of spindle-shaped cellulose nanocrystals were measured, via TEM, to be 15 ± 8 nm by 195 ± 93 nm with an aspect ratio of ~13 (as shown in Figure S6a). The CNC aqueous suspension was sonicated for 10 min to increase its colloidal stability prior to use. Gelatin (GE, Knox brand (USA) obtained from local grocery), titanium diisopropoxide bis(acetylacetonate) (Aldrich), pyrrole (Aldrich), and $(NH_4)_2S_2O_8$ (Certified ACS) were received from standard suppliers.

Structural characterization: Powder X-ray diffraction (PXRD) patterns of the samples were recorded on a D8 Advance X-ray diffractometer. Scanning electron microscopy (SEM) images of the samples were obtained on a Hitachi S4700 electron microscope. Samples were prepared by attaching them to aluminum stubs using double-sided adhesive tape and sputter coating with Pt-Pd (8 nm). Polarized optical microscopy (POM) was performed with crossed polarizers on an Olympus BX41 microscope. Energy-dispersive X-ray (EDX) analysis was collected using a Hitachi S2300 scanning electron microscope. Thermogravimetric analysis (TGA) of the samples (~10 mg) were conducted at a heating rate of 20 °C min^{-1} under air atmosphere from RT to 800 °C using a PerkinElmer Pyris 6 thermogravimetric analyzer. Infrared spectra were obtained on neat samples using a Nicolet 6700 FT-IR equipped with a

Smart Orbit diamond attenuated total reflectance (ATR) attachment. XPS measurements were achieved in an ion-pumped chamber (evacuated to 10^{-9} Torr) of a photoelectron spectrometer (Leybold MAX200) equipped with a focused Al Kα X-ray source. Gas adsorption experiments were conducted on a Micromeretics Accelerated Surface Area & Porosity (ASAP) 2020 system. Samples (~120 mg) were degassed at 60-150 °C in vacuum for 4 h before measurements. The electrochemical measurements were performed with a two-electrode configuration using a Brinkmann PGSTAT12 Autolab potentiostat. The PPy/gCNC aerogel composite fibers were weighed and then soaked in a 0.01 M KCl aqueous solution for at least 20 h. Two pieces of symmetrical PPy/gCNC aerogel composite fibers, one piece of 110 mm-sized round Whatman filter paper, and 0.01 M KCl were used as electrodes, separator, and electrolyte, respectively. Stainless-steel collectors sandwiched two fibers with a filter paper separator, and they were placed in a Swagelok two-electrode cell.

2. Captures and Figures

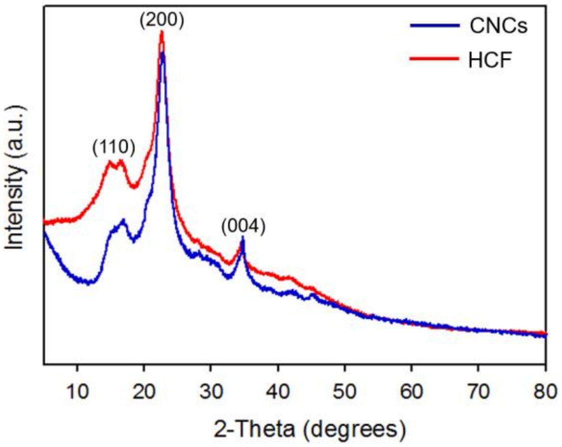

Figure S1. PXRD patterns of gelatin (GE)-crosslinked CNC (gCNC) aerogels (HCF) and pristine CNCs.

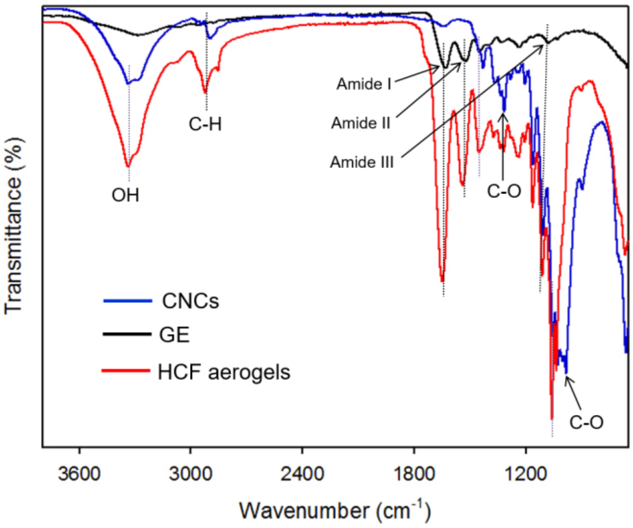

Figure S2. FTIR spectra of GE, CNCs, and HCF aerogels.

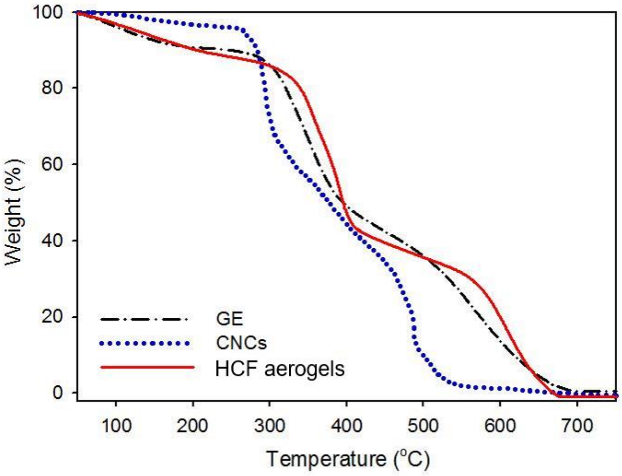

Figure S3. TGA curves of GE, CNCs, and HCF aerogels (20 °C min^{-1} under air atmosphere).

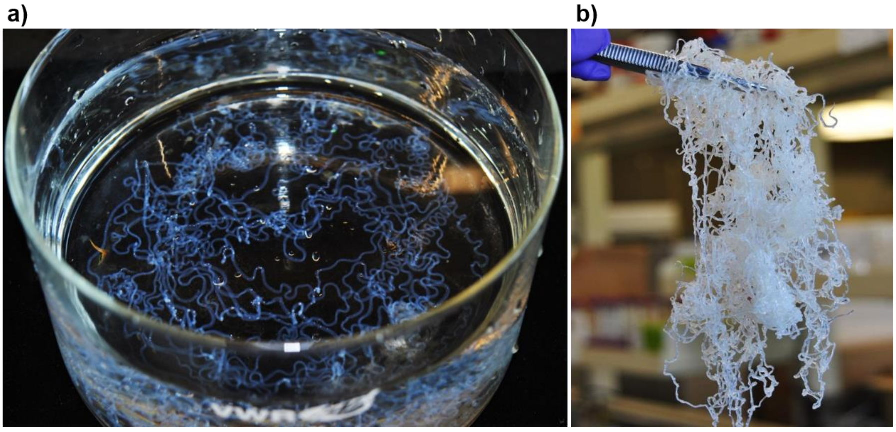

Figure S4. Photographs of (a) HCF hydrogels formed by injecting the GE/CNC aqueous mixtures into a water bath and (b) hydrogel fiber products collected from water. The fibers resemble cooked spaghetti.

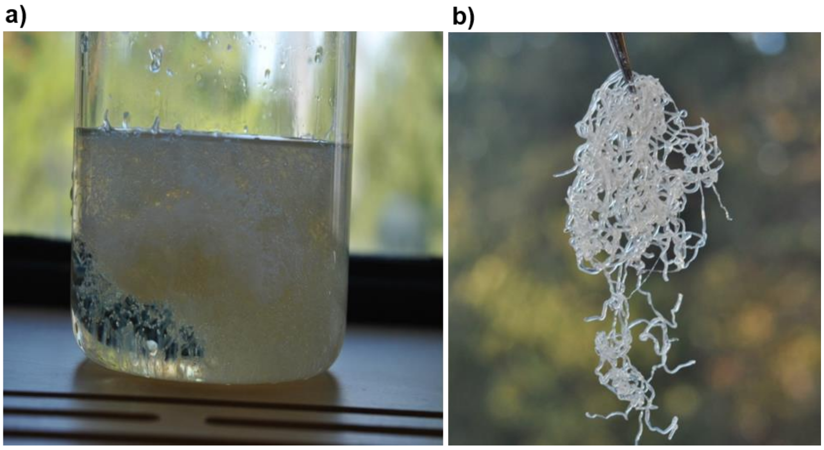

Figure S5. Photographs of (a) HCF alcogels immersed in ethanol and (b) alcogel fiber product collected from ethanol.

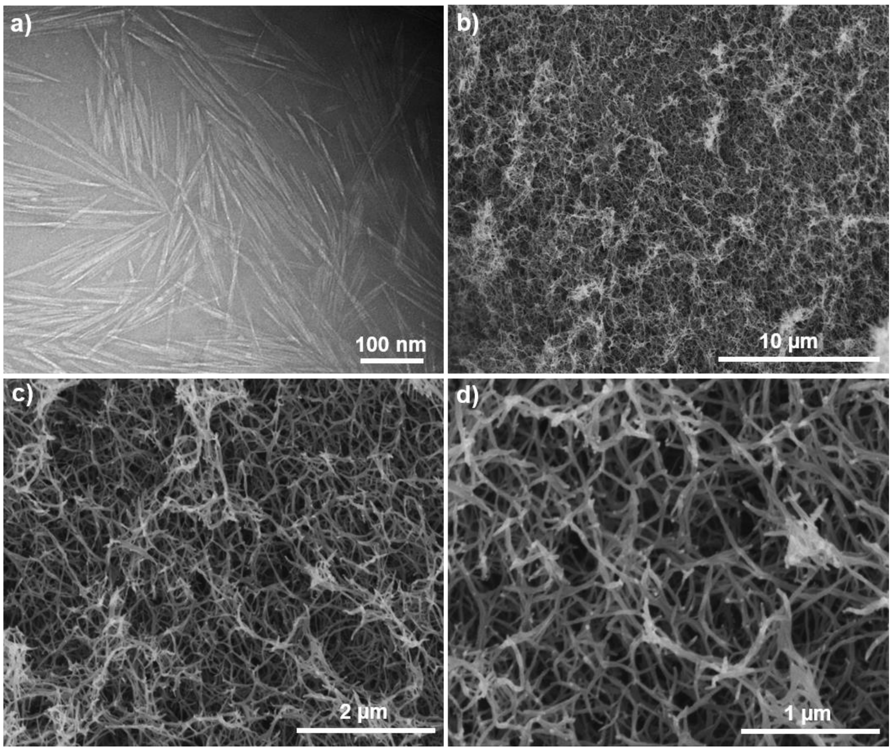

Figure S6. (a) TEM image of CNCs prepared from a highly dilute (0.002 wt%) CNC aqueous suspension and (b-d) Expanded SEM images of HCF aerogels at three different magnifications.

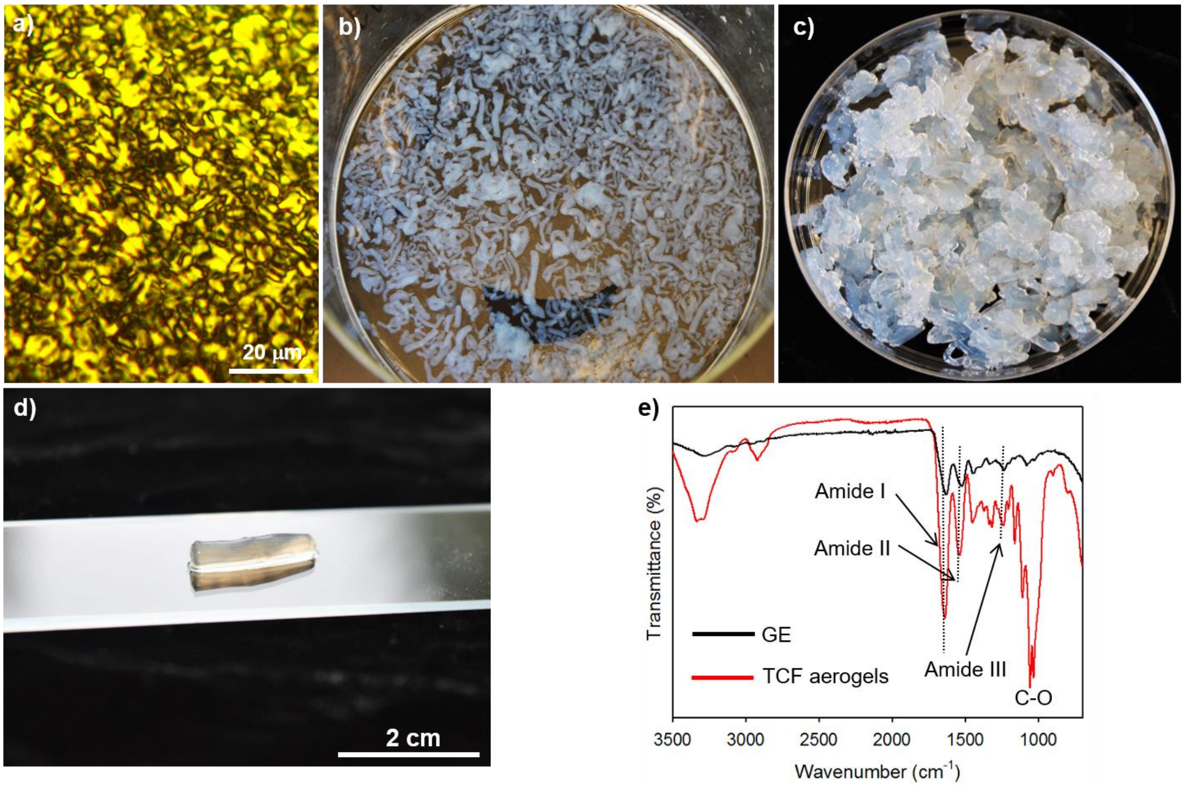

Figure S7. TCF hydrogels prepared by injecting ~10 wt% CNC aqueous suspension in 6 wt% GE aqueous solution followed by aging at 50 ^{o}C for 48 h. These fibers also resemble cooked spaghetti. (a) POM image of ~10 wt% CNC aqueous suspension prepared by water evaporation of dilute CNC suspension (~2.5 wt%, pH~6.5) in a Petri dish at ambient conditions showing a fingerprint texture characteristic of chiral nematic structure, (b) Photograph of TCF hydrogels formed in the GE aqueous solution, (c) Photograph of TCF hydrogels collected from the GE aqueous solution and washed through with warm water to remove GE adsorbed on the fiber's surfaces, (d) Photograph of a single TCF, and (e) FTIR spectra of TCF and GE.

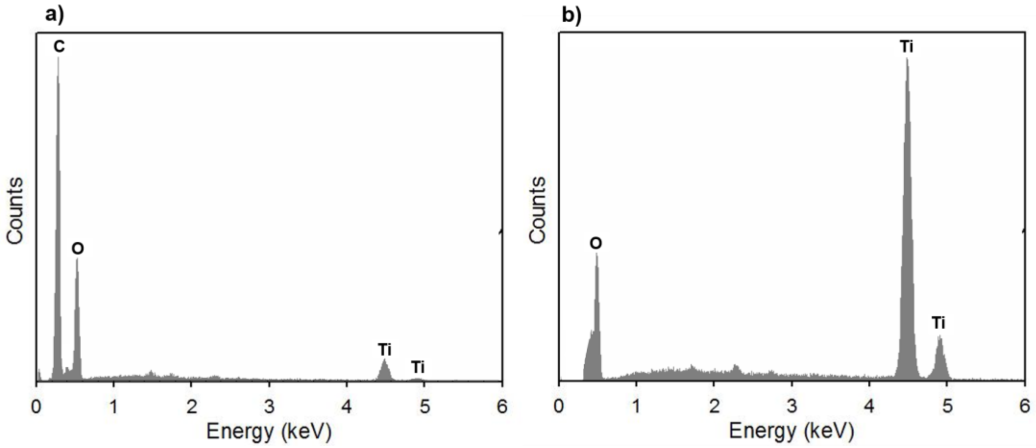

Figure S8. EDX spectra of (a) TiO_2/HCF aerogel composites and (b) calcined TiO_2 aerogels.

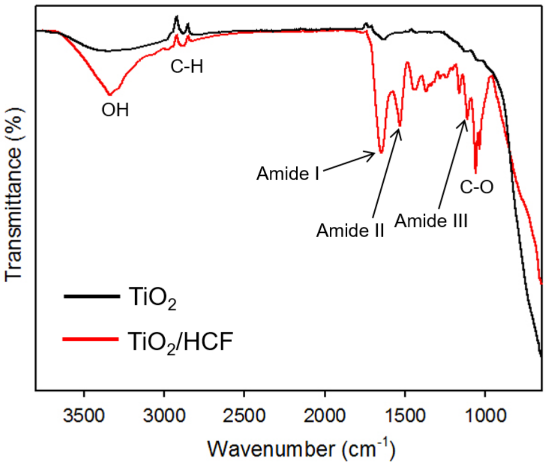

Figure S9. FTIR spectra of TiO_2/HCF aerogel composites and calcined TiO_2 aerogels.

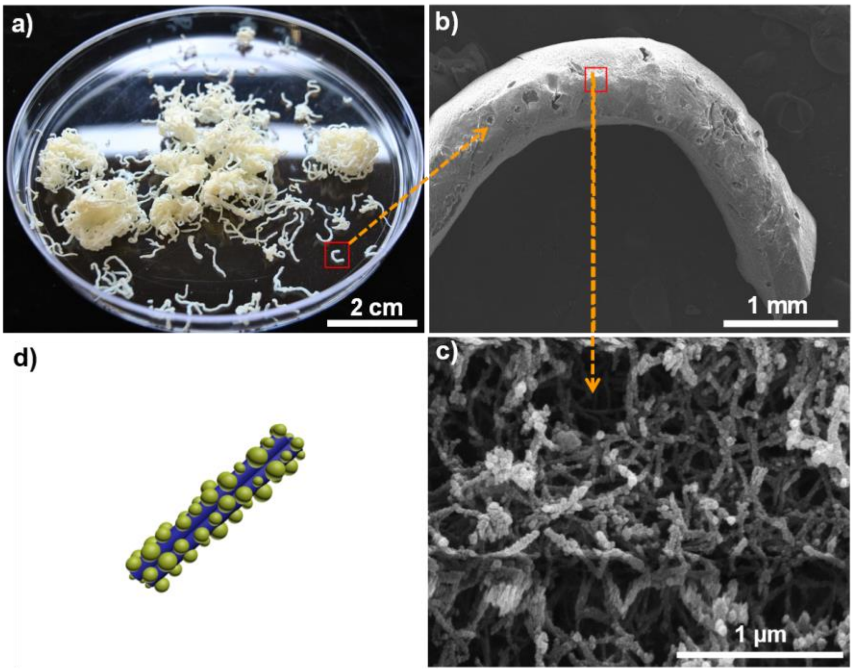

Figure S10. (a) Photograph and (b-c) expanded SEM images of TiO_2/HCF aerogel composites. (d) Model structure of a single TiO_2@gCNC nanorod bundle in the aerogel networks.

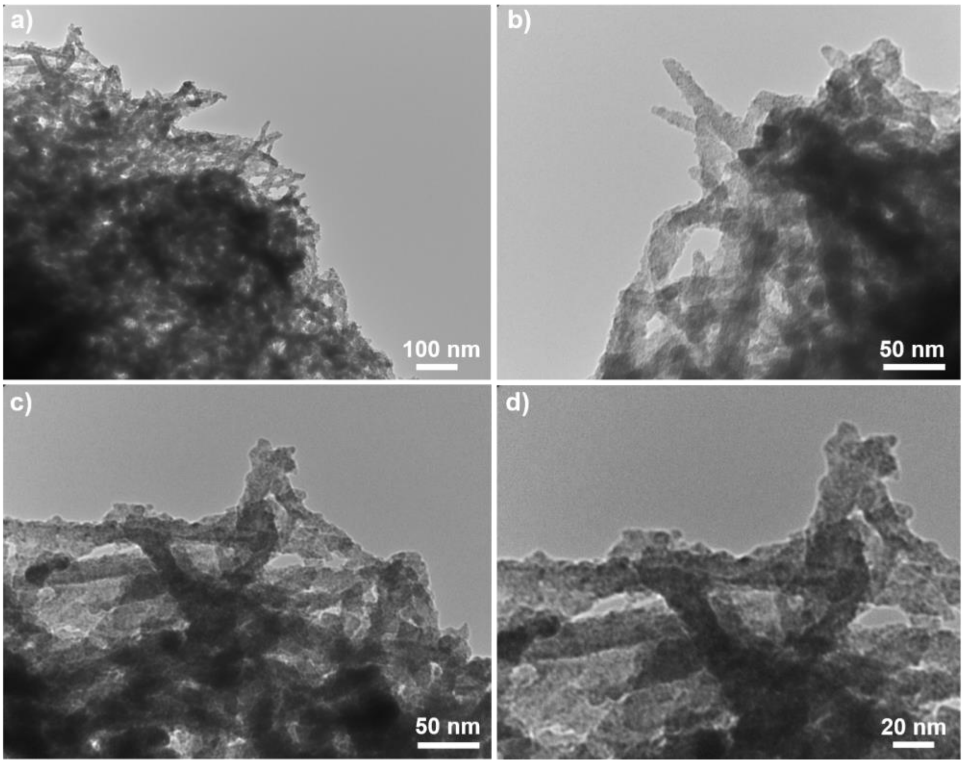

Figure S11. (a-d) Expanded TEM images of TiO_2/HCF aerogel composites (four different magnifications shown).

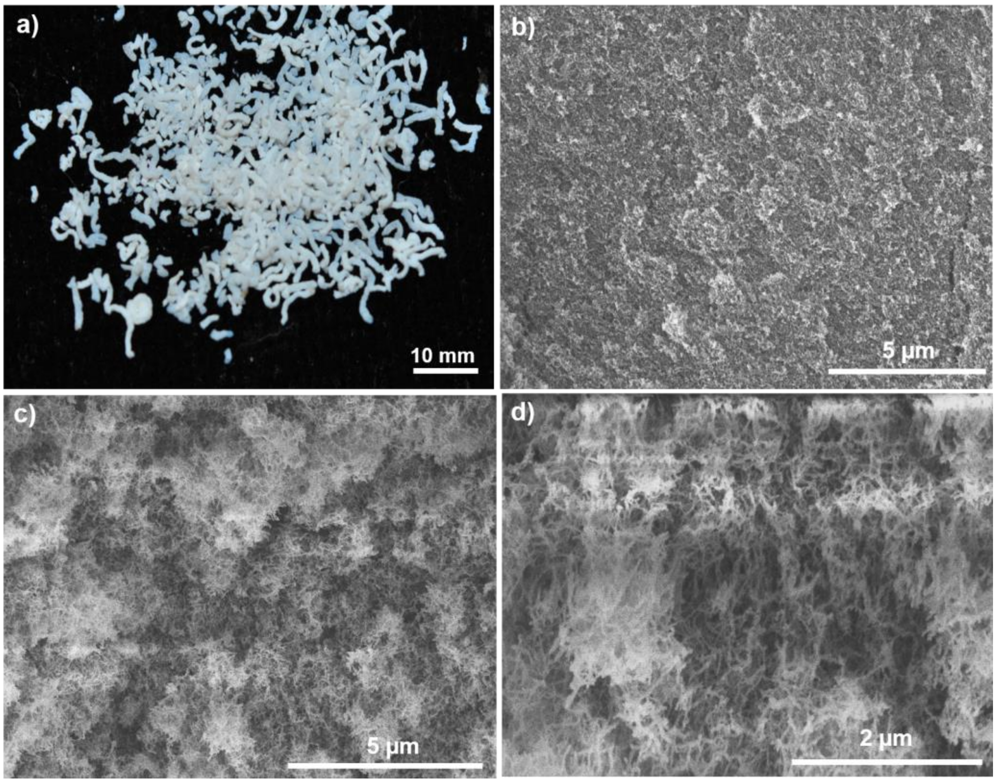

Figure S12. (a) Photograph and (b-d) Expanded SEM images of TiO_2 aerogel fibers obtained after thermal removal of HCF template in the composites (three different magnifications shown).

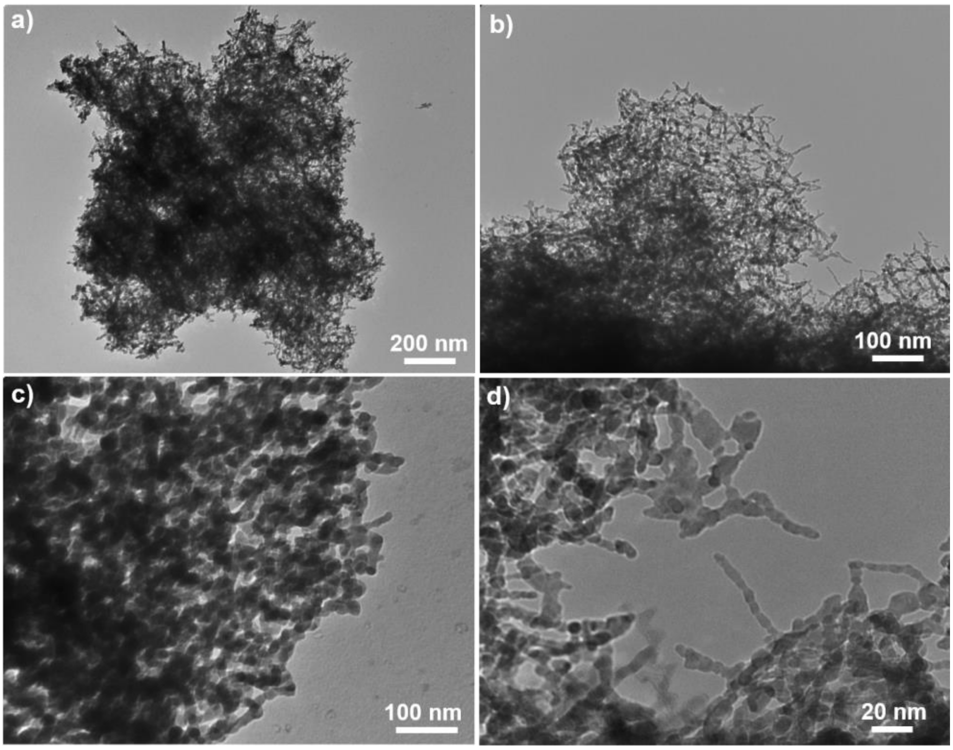

Figure S13. (a-d) Expanded TEM images of TiO_2 aerogel fibers after removal of HCF template (four different magnifications shown).

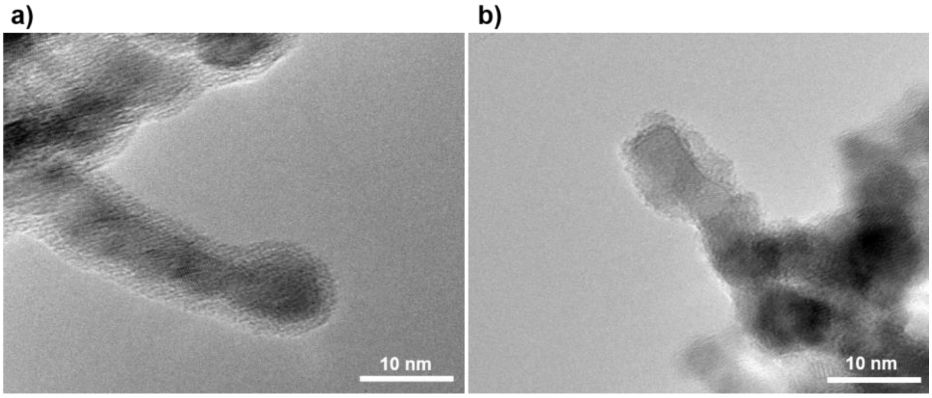

Figure S14. (a,b) Expanded HRTEM images of TiO_2 aerogel fibers after removal of HCF template.

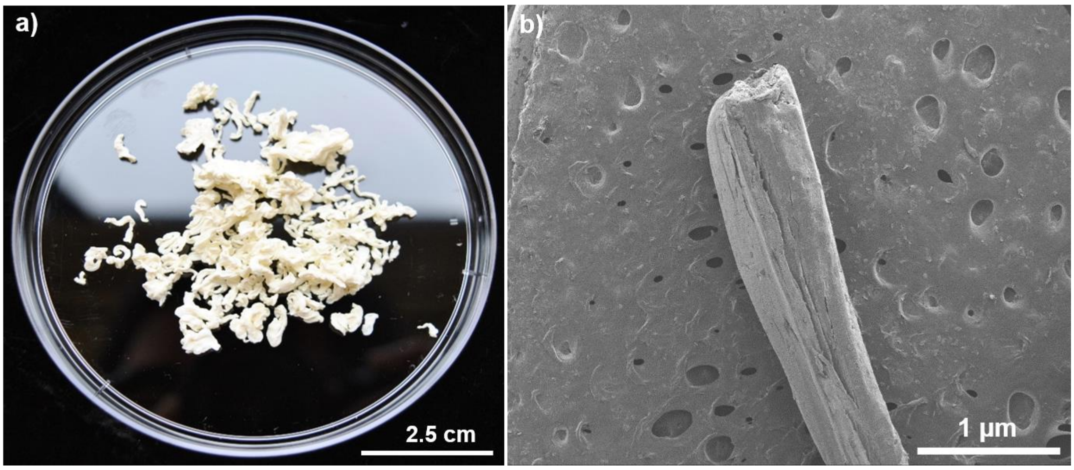

Figure S15. (a) Photograph and (b) low-magnification SEM image of TiO_2/TCF aerogel composites.

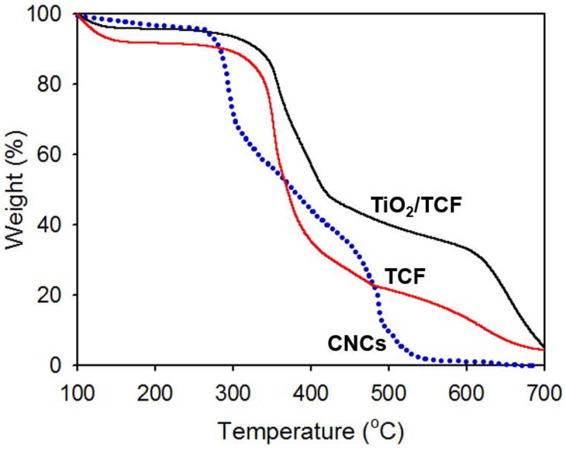

Figure S16. TGA curves of gCNC (TCF) and TiO_2/TCF aerogel composites compared with pristine CNCs (20 °C min^{-1} under air atmosphere). Thermal analyses show that TCF first dehydrated at below 250 ^{o}C and then started to decompose at about 320 ^{o}C that is higher than that of pristine CNCs (at ~290 ^{o}C). This indicates interactions between CNCs and GE to form the gel networks leads to the increased thermal stability.

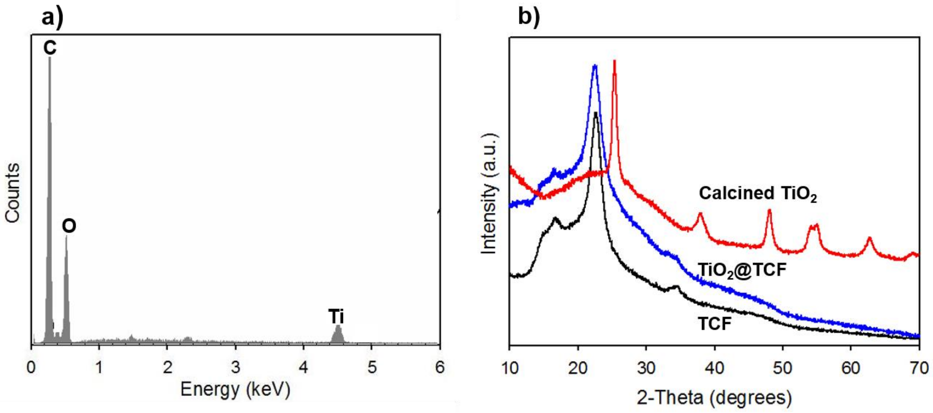

Figure S17. (a) EDX spectrum of TiO_2/TCF aerogel composites and (b) PXRD patterns of gCNCs (TCF), TiO_2/TCF aerogel composites, and calcined TiO_2 aerogels.

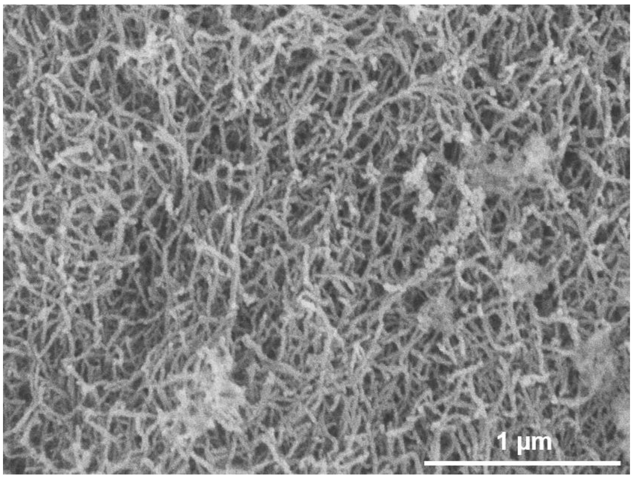

Figure S18. SEM image of TiO_2 nanofibrillar aerogels obtained from the direct calcination of TiO_2/TCF aerogel composites under air at 540 ^{o}C.

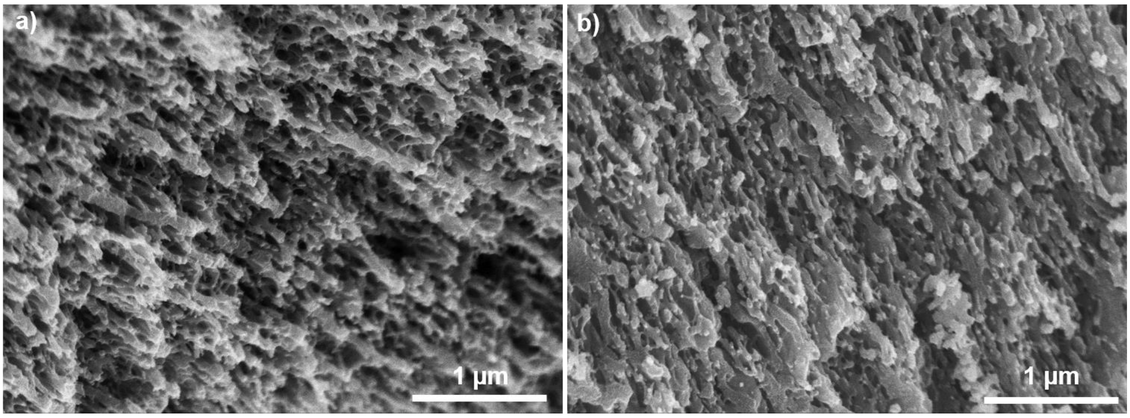

Figure S19. (a,b) SEM images of TiO_2/carbon nanofiber aerogels prepared by carbonizing TiO_2/TCF aerogel composites under nitrogen at 540 °C for 6 h.

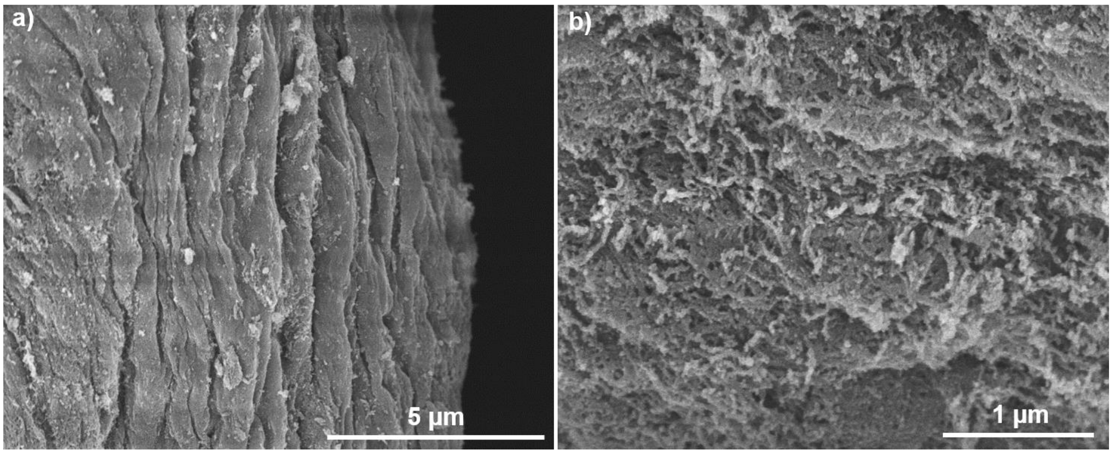

Figure S20. SEM images of layered TiO_2 nanofibrillar aerogels at (a) low and (b) high magnifications prepared by calcining the resulting TiO_2/carbon composites under air at 540 °C for 6 h.

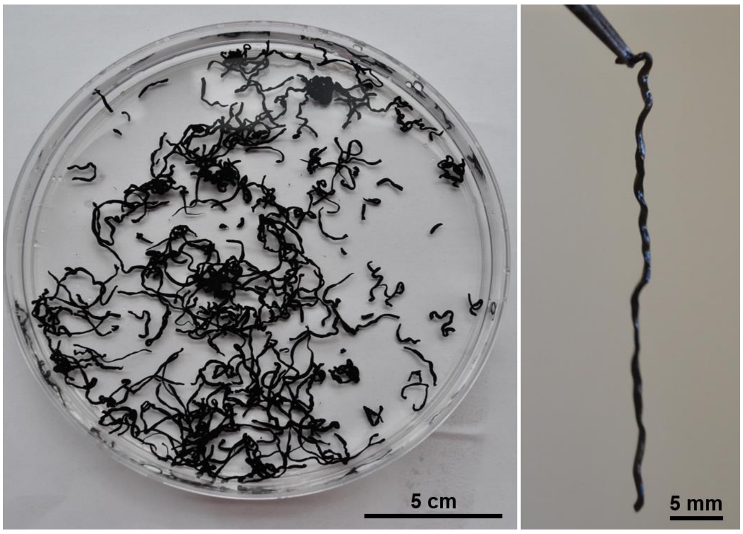

Figure S21. Photographs of PPy/HCF hydrogel composites stabilized in water.

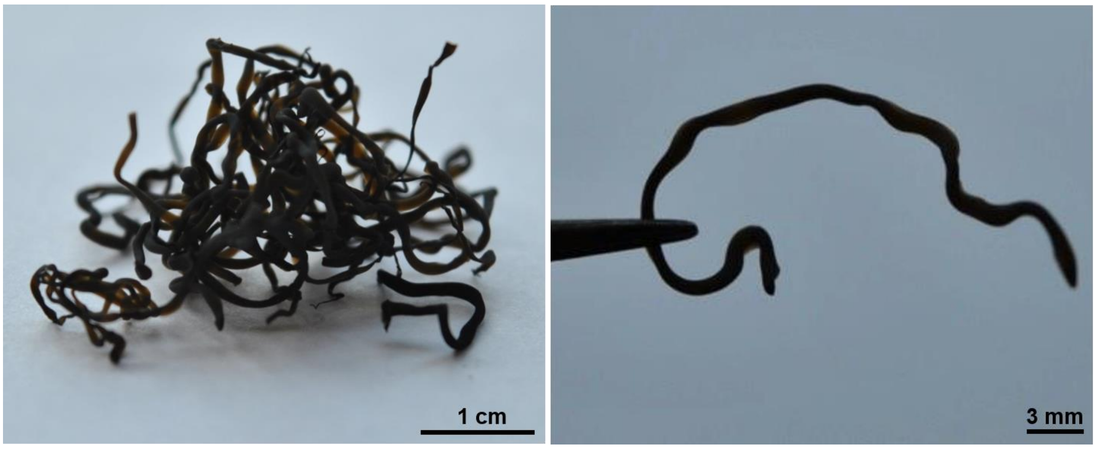

Figure S22. Photographs of PPy/HCF aerogel composites obtained after supercritical CO_2 drying of hydrogels.

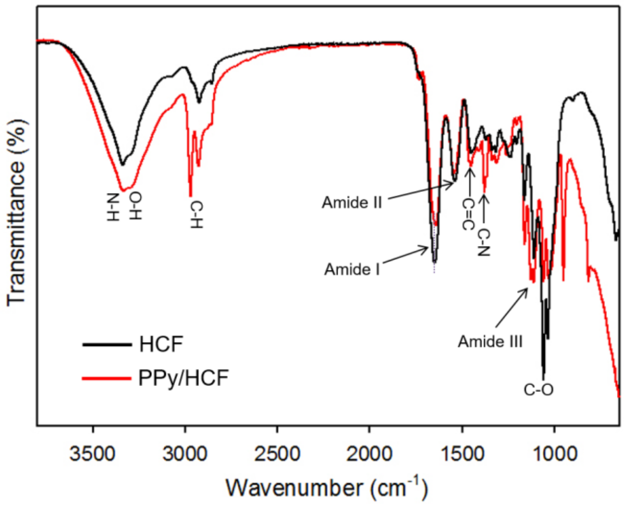

Figure S23. FTIR spectra of PPy/HCF aerogel composites in comparison with gCNC aerogels show specific stretching modes of C=C at ~1440 cm^{-1} and C-N at ~1380 cm^{-1} of polypyrrole in the composites, while these modes are absent from gCNCs.

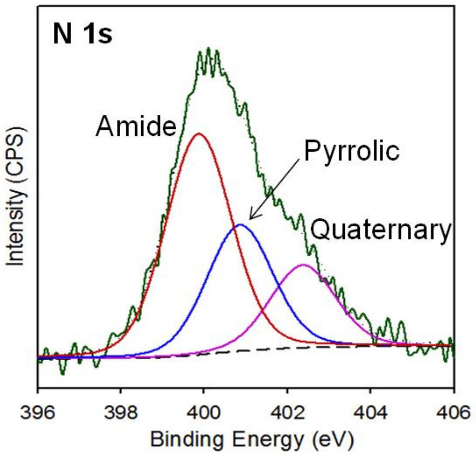

Figure S24. Deconvoluted N 1s XPS spectrum of PPy/HCF aerogel composites.

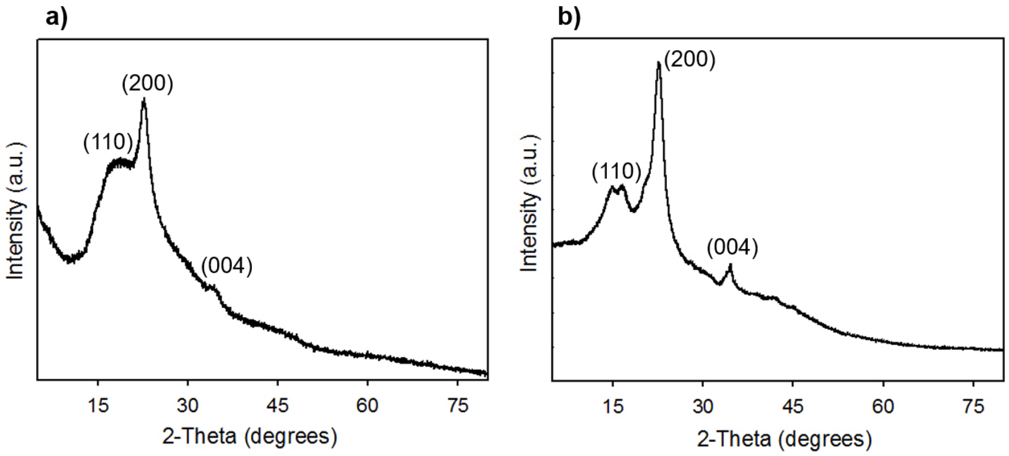

Figure S25. PXRD patterns of (a) PPy/HCF aerogel composites in comparison with (b) gCNC aerogels.

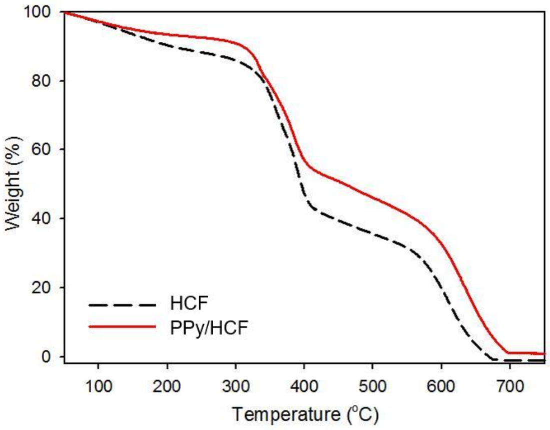

Figure S26. TGA curves of HCF aerogels and PPy/HCF aerogel composites (20 °C min^{-1} under air atmosphere).

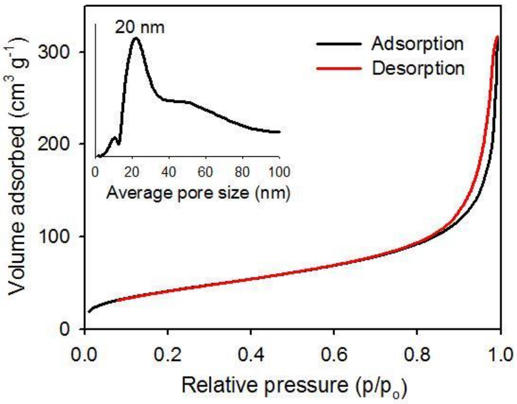

Figure S27. N_2 adsorption-desorption isotherms of PPy/HCF aerogel composites and inset of BJH pore size distribution.

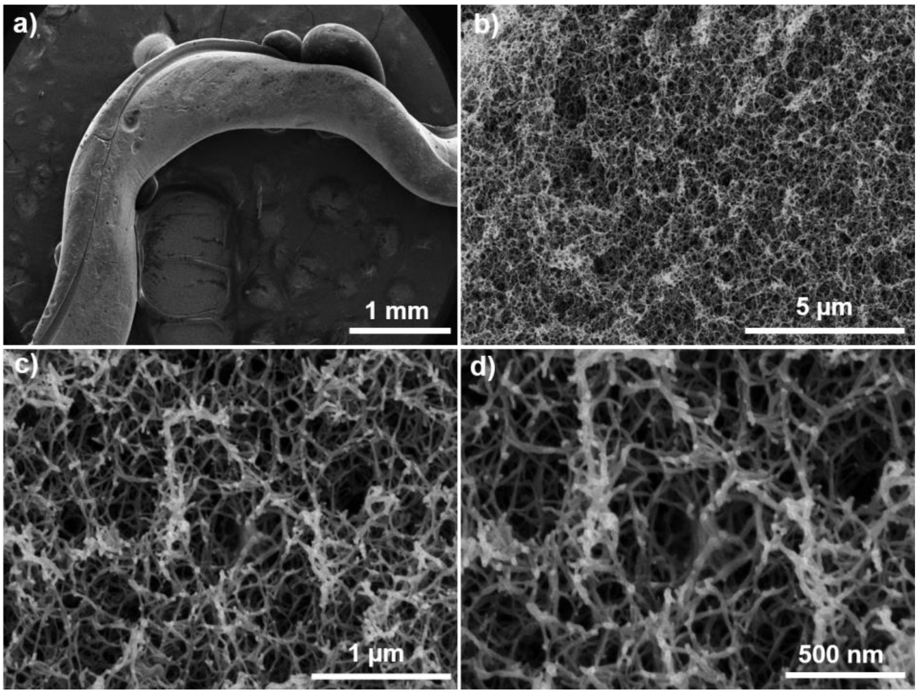

Figure S28. (a-d) Expanded SEM images of PPy/HCF aerogel composites (four different magnifications shown).

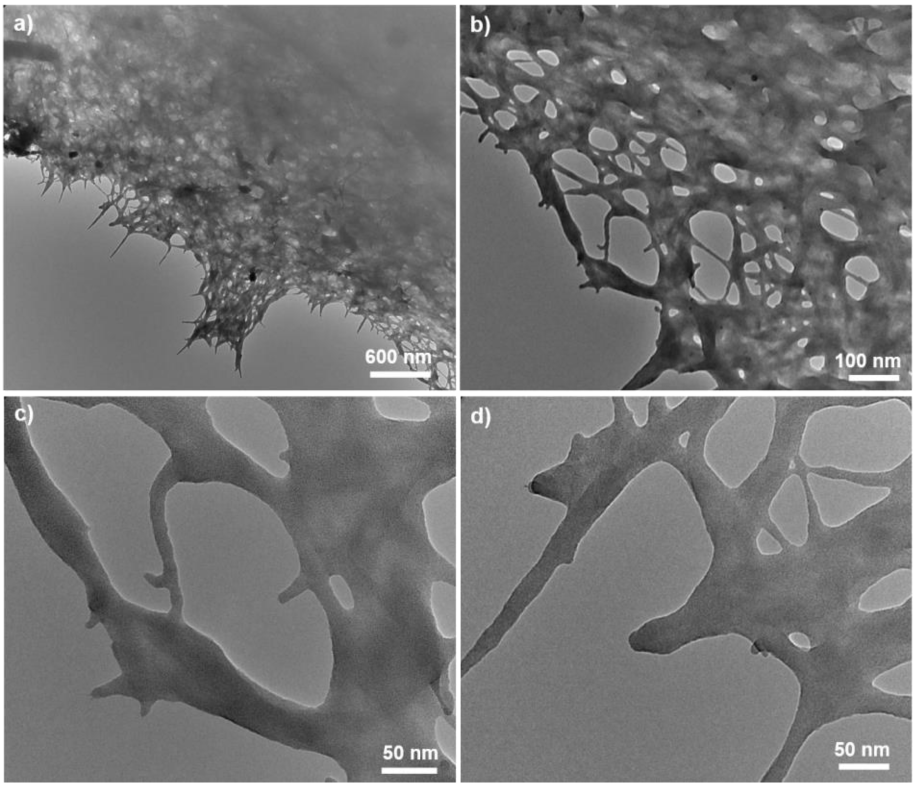

Figure S29. (a-d) Expanded TEM images of PPy/HCF aerogel composites (different magnifications shown).

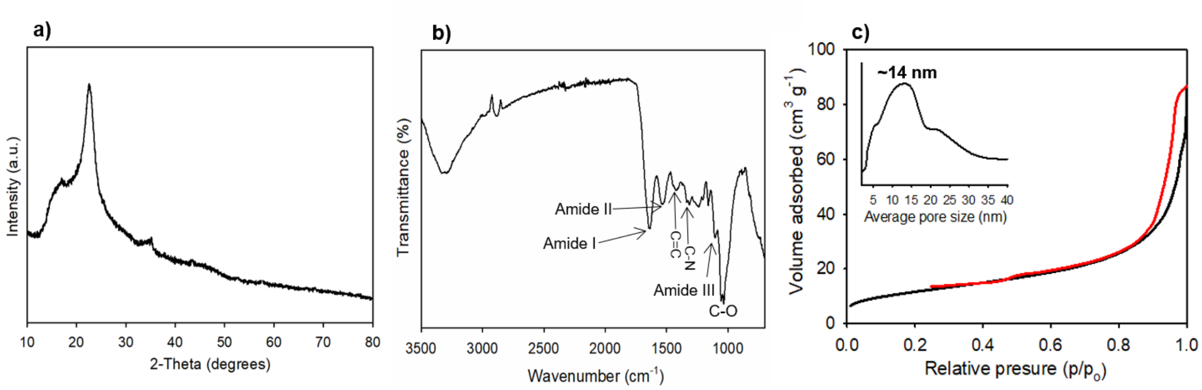

Figure S30. (a) PXRD pattern, (b) IR spectrum, and (c) nitrogen adsorption-desorption isotherms (inset of BJH pore size distribution) of PPy/TCF aerogel composites. Note that the chiral nematic structure led the PPy/TCF to have narrower pore size distribution than the PPy/HCF.

References

(1) K. E. Shopsowitz, H. Qi, W. Y. Hamad, M. J. MacLachlan, *Nature* **2010**, *468*, 422-425.

(2) W. Y. Hamad, T. Q. Hu, *Can. J. Chem. Eng.* **2010**, *88*, 392-402.